Lithuanian Journal of Physics, Vol. **62**, No. 3, pp. 127–137 (2022)

TOWARDS WIRELESS DATA TRANSMISSION WITH COMPACT ALL-ELECTRONIC THz SOURCE AND DETECTOR SYSTEM

A. Cesiul [a], K. Ikamas [a, c], D.B. But [b], I. Morkūnaitė [a], T. Lisauskas [d], and A. Lisauskas [a, b]

[a] *Institute of Applied Electrodynamics and Telecommunications, Vilnius University, Saulėtekio 3, 10257 Vilnius, Lithuania*
[b] *CENTERA Laboratories, Institute of High-Pressure Physics PAS, Sokołowska 29, 01-142 Warsaw, Poland*
[c] *Research Group on Logistics and Defense Technology Management, General Jonas Žemaitis Military Academy of Lithuania, Šilo 5A, 10322 Vilnius, Lithuania*
[d] *SE 'Terahertz Technologies', Pamėnkalnio 5-4, 01116 Vilnius, Lithuania*
Email: alvydas.lisauskas@ff.vu.lt

Received 17 September 2022; accepted 20 September 2022

This paper presents a fully-electronic wireless link operating at the 250 GHz frequency. The key elements of the developed system are the voltage-controlled harmonic oscillator implemented in 65 nm complementary metal-oxide-semiconductor technology (CMOS) and a quasi-optical detector with a resonant-antenna-coupled field-effect transistor completed in 90 nm CMOS. The source is optimized for the third harmonic emission at 252 GHz with radiated power reaching up to –11 dBm (decibels with reference to one milliwatt) level. The detector has a resonance maximum of 254 GHz with a bandwidth of 25% and a minimal optical noise equivalent power of 22 pW/$\sqrt{\text{Hz}}$. We employ an on-off keying technique for data coding and demonstrate digital signal transmission from 0.4 to 18 m distances. At 0.4 m distance and modulation frequency of 32 MHz, we achieve a 15.9 dB signal-to-noise ratio. The channel capacity of assembled communication link reaches 266 Mbit/s. However, it is limited by external electronic components – the amplifier and the modulator bandwidths. Implementing state-of-the-art high-frequency circuits should allow directly scaling the throughput to 10 Gbit/s.

Keywords: power generation, wireless communication, THz detection, RF chipset, Si CMOS

1. Introduction

The terahertz (THz) frequency range is characterized by a wide variety of phenomena and can be used in many fields, such as materials science, security technology and wireless communications [1, 2]. The advanced terahertz communication links at frequencies over 100 GHz, developed rapidly in recent years, open possibilities to achieve extremely large data transmission bandwidths reaching to multi-Gbps per channel [3, 4]. The telecommunication community has already identified and widely discussed the demand for such data rates. The deployment of commercial 5th generation mobile communication (or 5G) is already started in many countries since 2020. The future generation of high-speed mobile links (6G or even 7G) can be based on the THz frequency range [5]. Another big demand for high data rates comes from the short-range wireless communications (such as Wi-Fi) industry [6].

Higher carrier frequencies are expected to result in higher data rates. Notably, THz communication links have several advantages compared to other high-frequency rivals, such as being based on shorter infrared (IR) or optical wavelengths. In particular, free-space propagated THz signals are attenuated less by the atmosphere than IR beams under certain weather conditions, especially in fog or rain [7]. In addition, THz waves can pass through some opaque materials [8]. In 2020, the ratified standard IEEE 802.15.3d proposed a channel allocation near 300 GHz [9]. In 2019, the International Telecommunication Union (ITU) also identified

275 to 296 GHz as suitable for telecommunications [10]. Also, a portion of the microwave band of the radio spectrum, between 241 and 250 GHz, is internationally allocated to amateur radio and amateur satellite use [11].

Novel THz communication links employ different generation and detection techniques, for example, photonic-based or all electronic-based approaches with different compound semiconductor (GaAs, SiGe) or Si semiconductor devices [2]. The latter, the industrial mainstream complementary metal-oxide-semiconductor (CMOS) technology, is very promising due to its readiness for large-scale integration or implementation of power combining techniques using integrated array antennas for higher output power [12]. Si CMOS-based device has already shown good results in quasi-optical THz imaging systems as radiation detectors [13–15] and emitters [16, 17] exhibiting signal-to-noise ratio (SNR) with 62 dB in the direct detection regime for one Hz equivalent noise bandwidth [18]. The new terahertz generation and detection approaches were facilitated by local nonlinearities of field effect transistors, which can be used even above their cut-off frequency for a rectification [19] as well as for frequency up-conversion [20].

A variety of fast and efficient THz waves controlling components and devices, such as THz transmitters, receivers, passive optical elements and fast amplitude modulators, are needed to build a practical THz data transmission system. Currently, the most advanced silicon technologies already enable the fabrication of complex electronic circuits directly operating in the microwave frequency range and touching the bottom limit of the terahertz band [21–24]. The progress of transceivers – the core of any communication system – in the sub-100-GHz range has risen rapidly in the second decade of this century. The data rate of such devices recently reached 120 Gb/s [4]. Some devices reached more than 50 Gb/s even at 14 GHz [24]. However, methods and devices for fast data transmission using THz waves are still under development. Recently, the 300 GHz single-chip CMOS transceiver with 80 Gb/s data rate has been demonstrated [25]. Two years earlier than that, the 300 GHz and 105 Gb/s transmitter was developed [26]. Despite these outstanding achievements, the majority of recent THz transceivers and transmitters in CMOS have exhibited the date rate lower than 30 Gb/s [27–31].

Here, we report on a free space all-electronic THz communication system, which fully consists of antenna-integrated Si-CMOS field-effect transistors (TeraFETs) and is potentially capable of transmitting 10 GBit/s signals.

2. Devices

The key elements of the developed transmission system are the harmonic oscillator implemented in 65 nm CMOS and the detector implemented in 90 nm CMOS technology. The principles of operation of both devices and the combined performance as an optopair are in detail described elsewhere [18]. Here we direct our attention to additional peculiarities which are of importance for data transmission experiments. Both the detector and the source of radiation were assembled by using high resistivity silicon substrate lenses with 12 mm diameter and 6.8 mm height with an additional 500 μm spacer. The concept of the assembly is presented in Fig. 1(a), whereas their photographs are presented in Fig. 1(b). The printed circuit board (PCB) with pads for bonding wires are fixed to the *XY* translation stage which allows a fine adjustment of the device to the centre of hyper-hemispheric Si lens which is located at the centre of 30 mm cage system.

The voltage responsivity of the detector was measured with two THz sources independently. The power of sources was estimated using calibrated pyroelectric and optoacoustic THz power detectors. The resulting responsivity is presented in Fig. 2(a) for an electronic multiplier (a red line marked 'with electronic source') and a photomixer source (a blue line with symbols). The light grayed curve of the background shows the raw data from standing waves in the photomixer-based measurement system. The maximum responsivity is optimized for 254 GHz frequency, and a full-width-at-half-maximum bandwidth of about 25% with the details on the integrated antenna reported previously [32]. However, for fast data transmission experiments, we have modified the low-noise preamplifier circuit by selecting, to our knowledge, one of the fastest on the market available integrated circuits (IC) with FET input (*Texas Instruments* OPA858 with 5.5 GHz gain bandwidth). By this, we extended the modulation bandwidth from the previously reported 3 to 40 MHz – however, paying with the price in the increase of the 1/*f* noise corner frequency to about 4 kHz (see Fig. 2(b)). For the comparison,

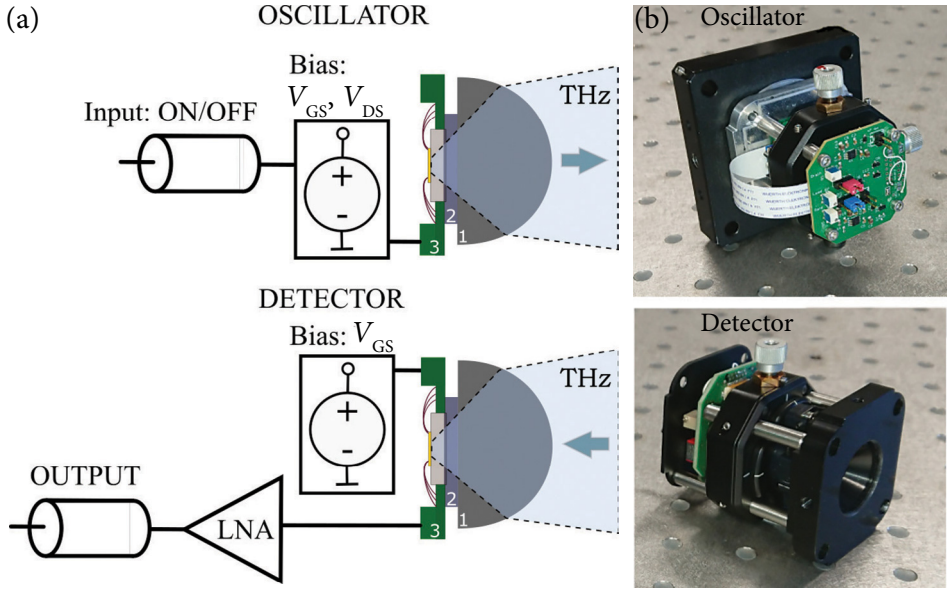

Fig. 1. (a) A simplified sketch for the oscillator (top) and detector (bottom) assemblies. The construction of both systems shares a similar concept and elements: a high resistivity silicon lens (denoted as 1) with 12 mm diameter and 6.8 mm height, a 500 μm thick undoped silicon substrate wafer (2) which is glued to the PCB (3) with bonding pads and protection electronics. The flat interface between the 1 and 2 components allows sliding the device over the lens centre. (b) Photos of packaged oscillator and detector modules utilized in the data transmission line. LNA, low-noise amplifier; V_{GS}, gate-source voltage; V_{DS}, drain-source voltage; PCB, printed circuit board.

our first implementation reported in Ref. 32 exhibits the 1/*f* noise corner frequency as low as 10 Hz. The main bandwidth limiting aspect can be attributed to the comparatively high impedance of the detector (usually about 4 kΩ), which in conjunction with the 1 pF input capacitance of IC exactly predicts the measured 40 MHz modulation bandwidth.

The spectral density of output voltage fluctuations presented in Fig. 2(b) also reveals three important frequency regimes. First, at low frequencies before

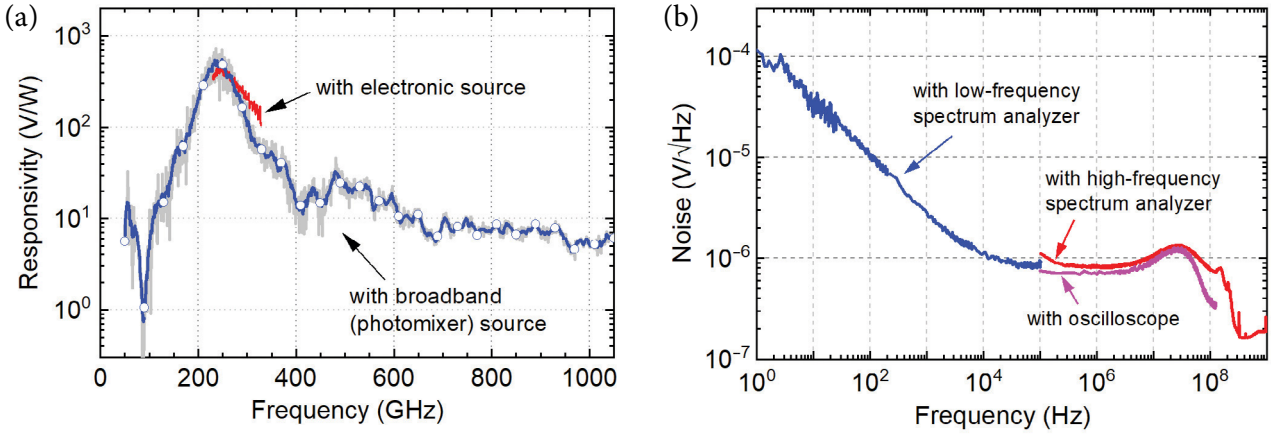

Fig. 2. (a) The responsivity of the detector was measured with two THz sources: an electronic multiplier (a red line) and a photomixer source (a blue line with symbols). The light grayed curve of the background shows the raw data from standing waves in the photomixer-based measurement system. (b) The spectrum of the spectral density of output voltage fluctuations. The frequency range from 1 Hz to 1 GHz was covered by combining measurements performed with several devices.

the so-called 1/*f* noise corner, a frequency output noise is dominated by 1/*f* noise. Second, in the intermediate frequency range up to about 40 MHz, the output noise is mainly determined by thermal fluctuations of the detector resistance at which the minimal optical noise-equivalent power (NEP) of 22 pW/$\sqrt{\text{Hz}}$ can be reached. Third, a weakly pronounced noise peak at higher frequencies originates from the current noise of amplifier circuitry. To not diminish the maximal possible signal-to-noise ratio (SNR) of the data transmission system, which is defined by the thermal noise of the detector, the high-frequency noise of components should be kept at a minimum.

Figure 3 presents two home-built setups implemented in order to determine the spectrum of CMOS sources. The harmonic content of the emission was investigated with a Michelson-type interferometer with a broadband detector [33], see Fig. 3(a). Whereas the high-resolution spectroscopy, as well as phase noise measurements, have been performed using the heterodyne setup presented in Fig. 3(b). The latter scheme is based on detecting a beat signal between the spatially overlapped radiation from the device under test (the CMOS emitter) and the frequency multiplied synthesized generator. This setup allows one not only to determine the dependence of the frequency of CMOS source oscillations but also to estimate its phase noise from the line-width of mixing signal at intermediate frequencies.

The amplitude of the Fourier transformed autocorrelation signal of the emitted spectrum is presented in Fig. 4(a). As designed, most power is concentrated in the 3rd harmonic at 256 GHz. However, many higher harmonics can be seen in the calculated spectrum. Most of them are believed to be the numerical artifacts of the analysis. The reflections cause these artifacts in the measurement setup. The impact of back-reflected radiation weakly depends on the emission strength of the source. Even two 8 dB attenuators did not completely suppress the harmonics, leaving the six and nine at 520 and 776 GHz. To be certain about the origin of spectral peaks at higher harmonics, it is necessary to carry out an additional experiment with resonant detectors in the vicinity of these frequencies.

The spectrum of the mixing signal at intermediate frequencies is presented in Fig. 4(b). Based on the analysis of the linewidth, we find that the phase noise at a 1 MHz distance from the central peak is as low as –80 dBc/Hz (i.e. dB/Hz relative to carrier) for the operation bias conditions (gate voltage 0.95 V an drain voltage 1.4 V),

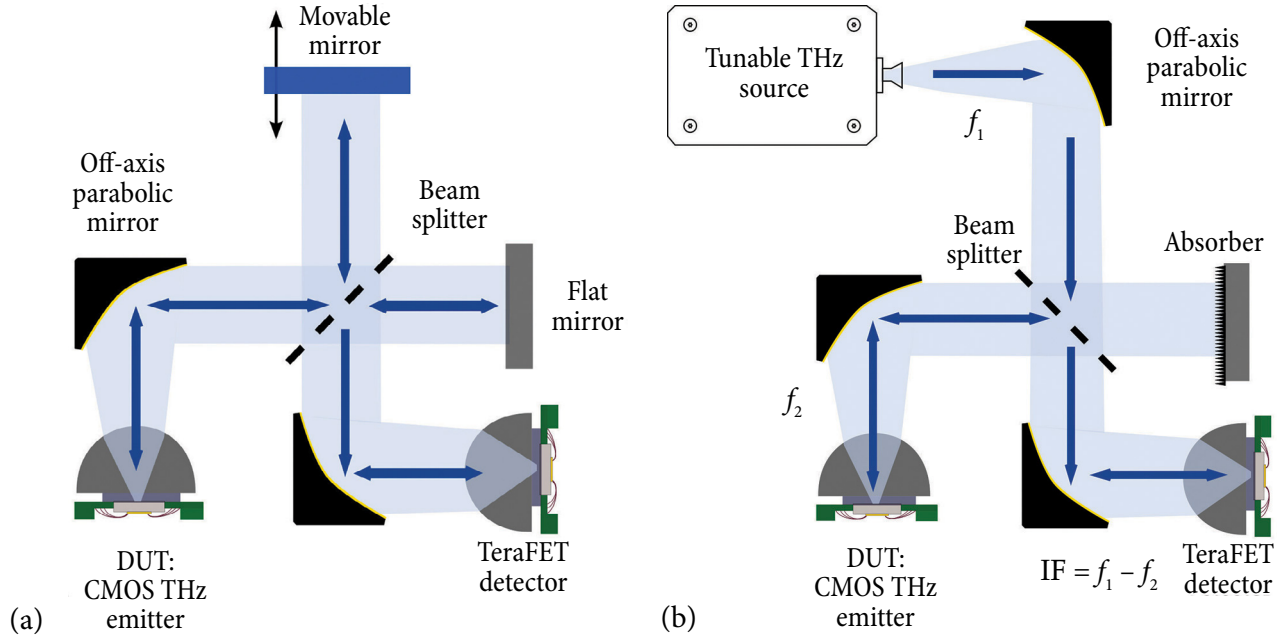

Fig. 3. Setups for determination of emitter radiation frequency. (a) A home-built Fourier transform interferometer with a broadband detector. (b) The heterodyne mixing setup with an additional source in the role of local oscillator. The radiation from the CMOS THz emitter (a device under test – DUT) is overlapped with the synthesized frequency multiplied source (a reference).

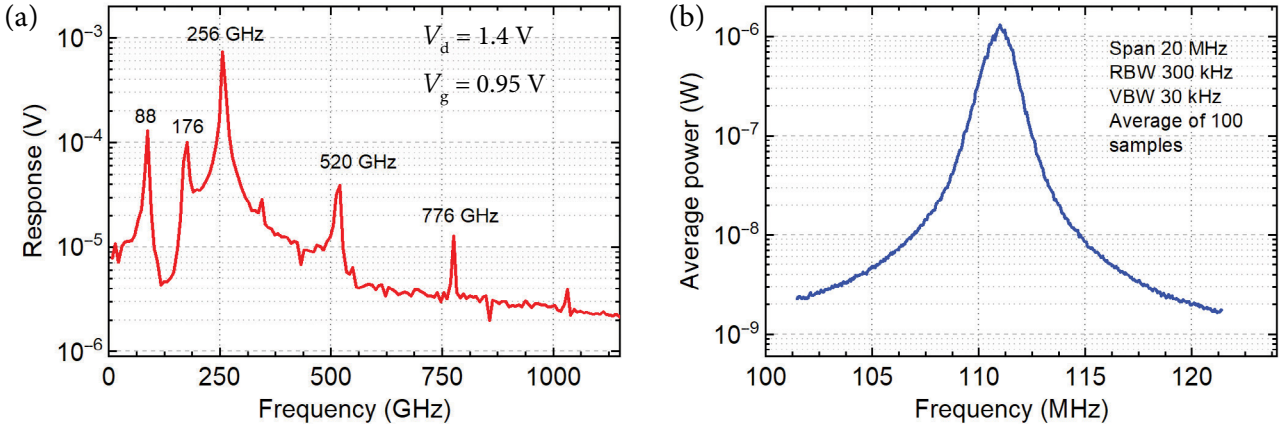

Fig. 4. (a) The CMOS THz emitter spectrum was measured with a Michelson-type interferometer. (b) The spectrum of the mixing signal at the intermediate frequencies was measured with a heterodyne setup. The gate voltage is 0.95 V, drain bias is 1.4 V.

which compares well with the state-of-the-art values reported for the comparable free-running voltage-controlled oscillators [34, 35].

3. Wireless digital data transmission link

The implemented point-to-point wireless data transmission link schematic is presented in Fig. 5. The bias conditions for the transmitter were set to have the optimized third harmonic emission at 252 GHz. The maximum radiated power of –11 dBm (decibels with reference to one milliwatt) has been measured with a calibrated power detector. Off-axis parabolic mirrors with two different reflected focal lengths (RFL) were used: ones with 4-inch RFL and 2-inch diameter for short data transmission distances up to 0.5 m, and mirrors with 6-inch RFL and 3-inch diameter for longer distances up to 18 m. A system with larger aperture mirrors has lower power losses at longer distances.

Since the implemented control circuit of the source currently allows only an on/off keying scheme, a Raspberry Pi Pico microcontroller was used for data coding. The maximum bandwidth of the data stream using the serial peripheral interface (SPI) of the microcontroller is 32 Mb/s. The data stream consisted of the 'Hello World' text message encoded with ASCII (abbreviated from the American Standard Code for Information Interchange). The detected and demodulated data stream was recorded and analysed from the time traces taken by a Tektronix TBS 1072B oscilloscope.

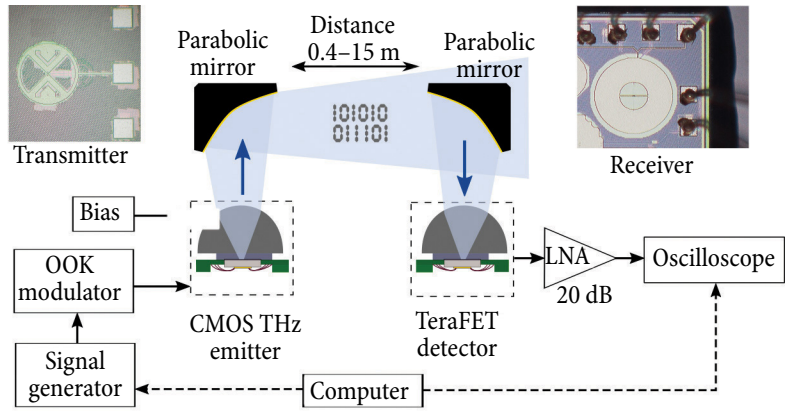

Fig. 5. The point-to-point data transmission line. The top left: the die micrograph of the transmitter, the core area is 305 × 220 μm. The top right: the micrograph of the receiver chip, the antenna area is 452 × 452 μm. Abbreviations: OOK, on-off keying; LNA, low-noise amplifier.

Additionally, we employed a pulse-width modulation scheme that allowed the live transmission of audio signals using 252 GHz carrier frequency over the 1 m distance and served for demonstration purposes.

Figure 6(a, b) shows the spatial THz beam profiles at the focal point of the second 6" off-axis parabolic mirror at the line-of-sight. The distance between the collimating and focusing mirrors was 4.8 m. The profiles were recorded in *Y* and *Z* directions (a) and *X* and *Y* directions (b). We used our 250 GHz detector with a smaller diameter (4 mm) Si lens and a two-axis motorized scanning stage for beam profile measurements. The resolution step of the scan was 0.5 × 0.5 mm^2.

The measurement in the *YZ* plane was allowed to determine the optimal distance between the detector and the last mirror – around 16 cm (Fig. 6(a)). The difference between the experimental value and the reflected focal point can be explained with an additional silicon substrate lens used to focus the THz beam tightly onto the TeraFET antenna [36] and a slightly greater distance between the emitter and the first mirror (13 cm instead of 12.5 cm). The last feature minimizes the beam propagation losses due to the natural Gaussian beam divergence. We scanned the beam profile in the *XY* plane near the optimal distance between the detector and the mirror. As expected, the detected radiation shape is close to the Gaussian shape intensity distribution perpendicular to the propagation direction (Fig. 6(b)). According to the measurement, the beam diameter of radiation *w* at half-power (–3 dB) points is 3 mm at a 16.5 cm distance from the second mirror.

4. Analysis of wireless link capacity

Figure 7 presents six open eye diagrams constructed from the recorded signal traces modulated by 1, 4, 8, 12 and 16 MHz, and with maximal for the controller frequency of 32 MHz. An eye diagram is a common indicator of the quality of signals in high-speed digital transmissions [37]. A distortion of the signal waveform due to intersymbol interference, and the noise appears as the eye pattern's closure.

For the evaluation of link capacity, here we focus on the SNR defined as a ratio between the peak-to-peak quantities of received signal amplitude and noise, or between the averaged signal power *S* and noise power *N*. The SNR, signal modulation bandwidth *B* and channel capacity *C* of a communication channel are connected by the Shannon–Hartley theorem:

$$C = B \cdot \log_2 (1 + \mathrm{SNR}). \tag{1}$$

The measured SNR at 1 MHz modulation frequency is 20 dB but drops to 15.9 dB at 32 MHz which is the maximal modulation frequency of our controller. The capacity of the assembled wireless data transmission link with *B* = 40 MHz and SNR = 100 can be estimated to reach 266 Mbit/s. It is important to note that there is a difference between the SNR obtained in direct power detec-

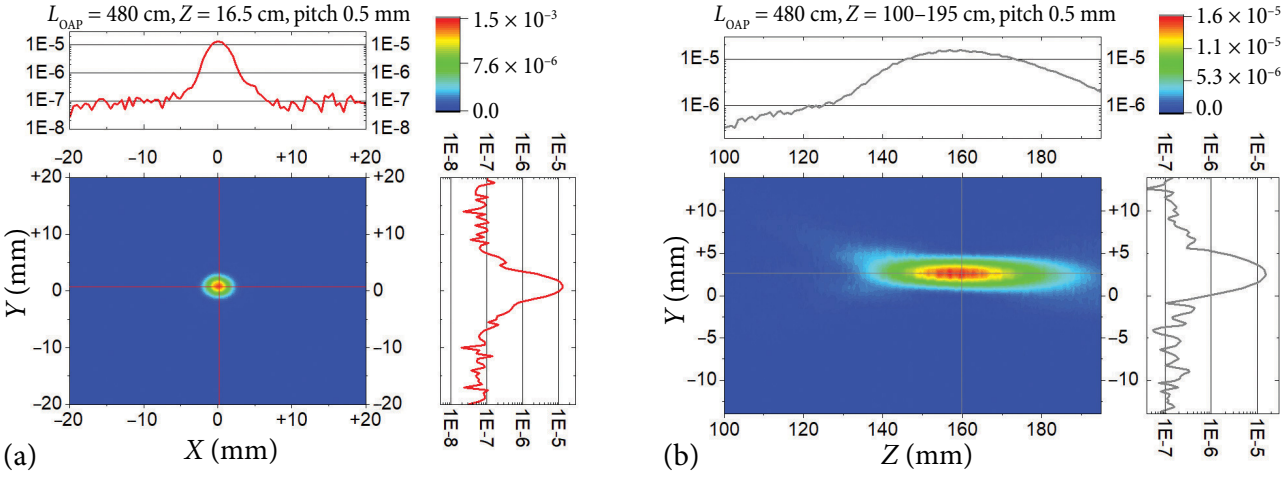

Fig. 6. The beam profiles in *YZ* plane (a) and *XY* plane (b) at the focal point of the last 6" off-axis parabolic mirror. The distance between mirrors L_{OAP} is 4.8 m. *Z* is the detector distance to the second mirror.

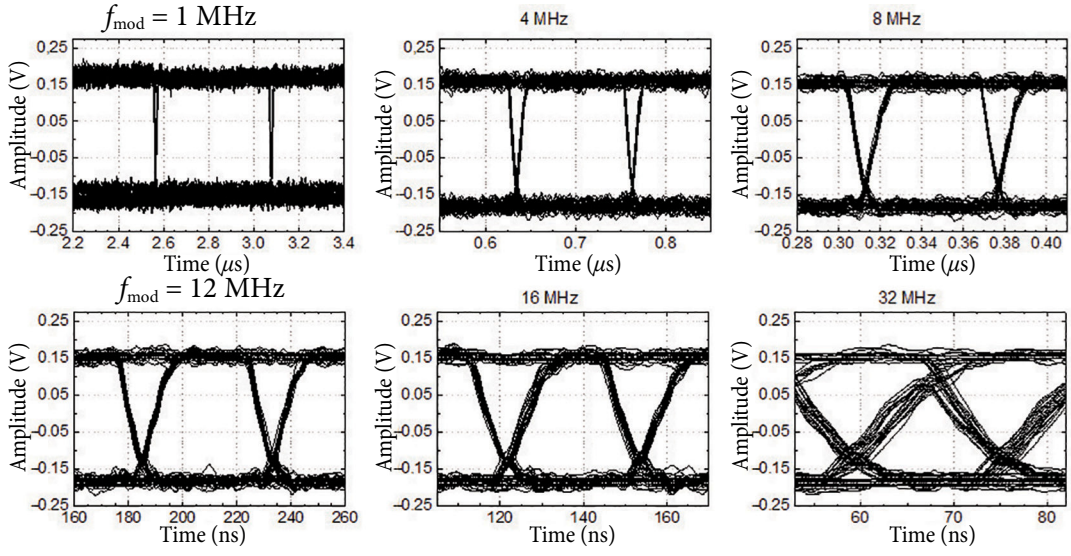

Fig. 7. The eye diagrams of the detector output signal for different modulation frequencies.

tion and heterodyne (which is often used in wireless communication links) detection schemes. For example, for the noise with frequency-independent spectral components or 'white' noise, the SNR of a heterodyne receiver is inversionally proportional to signal bandwidth B. While using the power detection scheme, SNR depends on $1/\sqrt{B}$. This difference also reflects in the calculations of theoretical channel capacity in the so-called power-limited case (SNR $\ll$ 1), i.e. $C \approx 1.44 \cdot B \cdot$ SNR. Using the heterodyne receiver mode, it becomes independent of the bandwidth and results in $C \approx 1.44 \cdot S/N_0$ with N_0 being defined as the spectral density of white noise power in Watts per Hertz. With the maximal achieved mixing signal of 10 dBm (10 mW) and the spectral density of noise power of –110 dBm/Hz (determined by the measured spectral density of voltage fluctuations of 1 μV/$\sqrt{\text{Hz}}$ in the 50 Ω output), the power-limited capacity of this link can be expected to reach $1.44 \cdot 10^{12}$ Bit/s. For the bandwidth limiting situation $C \approx 3.32 \cdot B \log_{10}$ SNR and C = 584 MBit/s for N = –34 dBm – not much differing from the achieved channel capacity in a direct power detection scheme. From this analysis, one can come to a straightforward conclusion that further improvement of practical communication links requires an increase in bandwidth without producing additional high frequency noise. With the cut-off frequencies for the 65 nm CMOS devices exceeding 100 GHz [18], it is feasible to expect the link

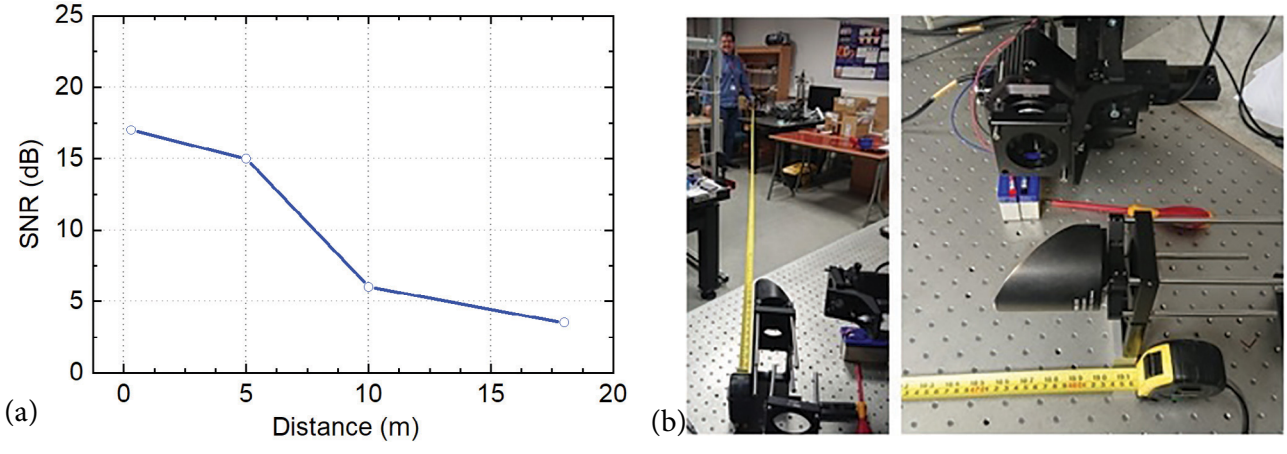

Fig. 8. (a) The transmission system SNR dependence on the line length. The modulation frequency is 20 MHz. (b) The photo of the 5 m data transmission setup. The detector module with the last 6" focal length off-axis mirror can be seen.

operation without bandwidth limitation at 10 GHz modulation frequencies. Another challenge for implementing practical high data rate systems poses the so-called signal path loss. To some extent, it can be compensated by increasing the directivity of used optical components; eventually, the power will be lost due to absorption and non-collinear beam propagation.

The data signals were transmitted at 40 cm, 5 m, 10 m and 18 m distances, with the main results for modulation at 20 MHz frequency summarized in Fig. 8(a). We achieve comparable SNR for the range from 0.4 to 5 m; for higher distances, it starts strongly decreasing due to beam divergence.

Finally, although we did not use equipment allowing for GBit/s signal transmission and detection, we give an indirect proof that our system is capable of competing with other state-of- the-art systems, which already proved to be able to transmit 10 GBit/s signals [20].

5. Conclusions

In this work, we report on a free space all-electronic THz communication system, which consists of antenna-integrated Si-CMOS field-effect transistors. The transmitter (TX) is based on a voltage-controlled two field-effect transistors-based differential Colpitts oscillator coupled with a resonant, slot-type antenna. It is optimized for the third harmonic emission at 252 GHz. The maximum radiated power is –11 dBm. The receiver (RX) is a resonant-antenna-coupled FET quasi-optical detector with a substrate lens. It has a resonance maximum of 254 GHz with a bandwidth of about 25% and a minimal optical NEP of 22 pW/$\sqrt{\text{Hz}}$. We employ an on-off keying technique of TX and a self-made low-noise amplifier on the RX side. The system demonstrates a signal-to-noise ratio of 15.9 dB at a 32 MHz modulation frequency and a channel capacity of 266 MHz. The data transmission speed in the current system is limited by used external electronic components – the LNA and the modulator. However, according to the Shannon–Hartley theorem, the theoretical information capacity of the system without bandwidth limitation based on our core CMOS elements could be at least 100 Gbit/s per channel. Implementing state-of-the-art transmitter circuits should allow directly scaling the throughput to 10 Gbit/s.

Acknowledgements

The Lithuanian team acknowledges funding from the Lithuanian Agency for Science, Innovation and Technology (MITA) Grant No. TPP-03-045. On the Polish side, the work was supported by the 'International Research Agendas' Programme of the Foundation for Polish Science, co-financed by the European Union under the European Regional Development Fund (No. MAB/2018/9) for CENTERA.

References

[1] R. Han, Z. Hu, C. Wang, J. Holloway, X. Yi, M. Kim, and J. Mawdsley, Filling the gap: Silicon terahertz integrated circuits offer our best bet, IEEE Microw. Mag. **20**(4), 80–93 (2019), https://doi.org/10.1109/MMM.2019.2891379

[2] T. Nagatsuma, Terahertz technologies: present and future, IEICE Electron. Expr. **8**(14), 1127–1142 (2011), https://doi.org/10.1587/elex.8.1127

[3] T. Nagatsuma, G. Ducournau, and C.C. Renaud, Advances in terahertz communications accelerated by photonics, Nat. Photonics **10**(6), 371–379 (2016), https://doi.org/10.1038/nphoton.2016.65

[4] K.K. Tokgoz, S. Maki, J. Pang, N. Nagashima, I. Abdo, S. Kawai, T. Fujimura, Y. Kawano, T. Suzuki, T. Iwai, K. Okada, and A. Matsuzawa, in: *Proceedings of 2018 IEEE International Solid-State Circuits Conference (ISSCC)* (2018) pp. 168–170, https://doi.org/10.1109/ISSCC.2018.8310237

[5] NTT Docomo, *White Paper: 5G Evolution and 6G (2021)* https://www.nttdocomo.co.jp/english/binary/pdf/corporate/technology/whitepaper_6g/DOCOMO_6G_White_PaperEN_v3.0.pdf

[6] C. Yi, D. Kim, S. Solanki, J.H. Kwon, M. Kim, S. Jeon, Y.C. Ko, and I. Lee, in: *Proceedings of 2020 International Conference on Information and Communication Technology Convergence (ICTC)* (2020) pp. 529–531, https://doi.org/10.1109/ICTC49870.2020.9289216

[7] L. Moeller, J. Federici, and K. Su, in: *Proceedings of 2011 XXXth URSI General Assembly and*

Scientific Symposium (2011) pp. 1–4, https://doi.org/10.1109/URSIGASS.2011.6050620

[8] K.B. Cooper, J.F. Trabert, and R.J. Dengler, in: *2012 IEEE/MTT-S International Microwave Symposium Digest* (2012) pp. 1–3, https://doi.org/10.1109/MWSYM.2012.6258431

[9] V. Petrov, T. Kurner, and I. Hosako, IEEE 802.15.3d: First standardization efforts for sub-terahertz band communications toward 6g, IEEE Commun. Mag. **58**(11), 28–33 (2020), https://doi.org/10.1109/MCOM.001.2000273

[10] The International Telecommunication Union (ITU), *Sharing and Compatibility Studies Between Land-mobile, Fixed and Passive Services in the Frequency Range 275-450 GHz* (2019), https://www.itu.int/pub/R-REP-SM.2450-2019

[11] *FCC Online Table of Frequency Allocations* (May 2019), https://transition.fcc.gov/oet/spectrum/table/fcctable.pdf

[12] R. Han and E. Afshari, A CMOS high-power broadband 260-GHz radiator array for spectroscopy, IEEE J. Solid-State Circuits **48**(12), 3090–3104 (2013), https://doi.org/10.1109/JSSC.2013.2272864

[13] J. Zdanevičius, K. Ikamas, J. Matukas, A. Lisauskas, H. Richter, H.-W. Hubers, M. Bauer, and H.G. Roskos, in: *Proceedings of 42nd International Conference on Noise and Fluctuations (ICNF)* (IEEE, 2017) pp. 1–4, https://doi.org/10.1109/ICNF.2017.7985960

[14] D.B. But, E. Javadi, W. Knap, K. Ikamas, and A. Lisauskas, in: *Proceedings of 2020 23rd International Microwave and Radar Conference (MIKON)* (IEEE, 2020) pp. 305–308, https://doi.org/10.23919/MIKON48703.2020.9253787

[15] E. Javadi, D.B. But, K. Ikamas, J. Zdanevičius, W. Knap, and A. Lisauskas, Sensitivity of field-effect transistor-based terahertz detectors, Sensors **21**(9), 2909 (2021), https://doi.org/10.3390/s21092909

[16] B. Khamaisi and E. Socher, A 209–233 GHz frequency source in 90 nm CMOS technology, IEEE Microw. Wirel. Compon. Lett. **22**(5), 260–262 (2012), https://doi.org/10.1109/LMWC.2012.2190272

[17] H. Jalili and O. Momeni, A 0.46-THz 25-element scalable and wideband radiator array with optimized lens integration in 65-nm CMOS, IEEE J. Solid-State Circuits **55**(9), 2387–2400 (2020), https://doi.org/10.1109/JSSC.2020.2989897

[18] K. Ikamas, D.B. But, A. Cesiul, C. Kołaciński, T. Lisauskas, W. Knap, and A. Lisauskas, All-electronic emitter detector pairs for 250 GHz in silicon, Sensors **21**(17), 5795 (2021), https://doi.org/10.3390/s21175795

[19] J. Zdanevičius, D. Čibiraitė, K. Ikamas, M. Bauer, J. Matukas, A. Lisauskas, H. Richter, T. Hagelschuer, V. Krozer, H.-W. Hubers, and H.G. Roskos, Field-effect transistor based detectors for power monitoring of THz quantum cascade lasers, IEEE Trans. Terahertz Sci. Technol. **8**(6), 613–621 (2018), https://doi.org/10.1109/TTHZ.2018.2871360

[20] N. Buadana, S. Jameson, and E. Socher, in: *Proceedings of 2018 IEEE Radio Frequency Integrated Circuits Symposium (RFIC)* (2018) pp. 248–251, https://doi.org/10.1109/RFIC.2018.8428967

[21] J. Pang, S. Maki, S. Kawai, N. Nagashima, Y. Seo, M. Dome, H. Kato, M. Katsuragi, K. Kimura, S. Kondo, et al., in: *Proceedings of 2017 IEEE International Solid-State Circuits Conference (ISSCC)* (2017) pp. 424–425, https://doi.org/10.1109/ISSCC.2017.7870442

[22] K. Okada, R. Minami, Y. Tsukui, S. Kawai, Y. Seo, S. Sato, S. Kondo, T. Ueno, Y. Takeuchi, T. Yamaguchi, A. Musa, R. Wu, M. Miyahara, and A. Matsuzawa, in: *2014 IEEE International Solid-State Circuits Conference Digest of Technical Papers (ISSCC)* (2014) pp. 346–347, https://doi.org/10.1109/ISSCC.2014.6757463

[23] S. Kawai, R. Minami, Y. Tsukui, Y. Takeuchi, H. Asada, A. Musa, R. Murakami, T. Sato, Q. Bu, N. Li, M. Miyahara, K. Okada, and A. Matsuzawa, in: *Proceedings of 2013 IEEE Radio Frequency Integrated Circuits Symposium (RFIC)* (2013) pp. 137–140, https://doi.org/10.1109/RFIC.2013.6569543

[24] P.-J. Peng, J.-F. Li, L.-Y. Chen, and J. Lee, in: *Proceedings of 2017 IEEE International Solid-State*

Circuits Conference (ISSCC) (2017) pp. 110–111, https://doi.org/10.1109/ISSCC.2017.7870285

[25] S. Lee, R. Dong, T. Yoshida, S. Amakawa, S. Hara, A. Kasamatsu, J. Sato, and M. Fujishima, in: *Proceedings of 2019 IEEE International Solid-State Circuits Conference (ISSCC)* (2019) pp. 170–172, https://doi.org/10.1109/ISSCC.2019.8662314

[26] K. Takano, S. Amakawa, K. Katayama, S. Hara, R. Dong, A. Kasamatsu, I. Hosako, K. Mizuno, K. Takahashi, T. Yoshida, and M. Fujishima, in: *Proceedings of 2017 IEEE International Solid-State Circuits Conference (ISSCC)* (2017) pp. 308–309, https://doi.org/10.1109/ISSCC.2017.7870384

[27] Z. Wang, P.-Y. Chiang, P. Nazari, C.-C. Wang, Z. Chen, and P. Heydari, A CMOS 210-GHz fundamental transceiver with OOK modulation, IEEE J. Solid-State Circuits **49**(3), 564–580 (2014), https://doi.org/10.1109/JSSC.2013.2297415

[28] Y. Yang, S. Zihir, H. Lin, O. Inac, W. Shin, and G.M. Rebeiz, in: *Proceedings of 2014 IEEE Radio Frequency Integrated Circuits Symposium* (2014) pp. 365–368, https://doi.org/10.1109/RFIC.2014.6851743

[29] S.V. Thyagarajan, S. Kang, and A.M. Niknejad, A 240 GHz fully integrated wideband QPSK receiver in 65 nm CMOS, IEEE J. Solid-State Circuits **50**(10), 2268–2280 (2015), https://doi.org/10.1109/JSSC.2015.2467216

[30] K.K. Tokgoz, S. Maki, S. Kawai, N. Nagashima, J. Emmei, M. Dome, H. Kato, J. Pang, Y. Kawano, T. Suzuki, et al., in: *Proceedings of 2016 IEEE International Solid-State Circuits Conference (ISSCC)* (2016) pp. 242–243, https://doi.org/10.1109/ISSCC.2016.7417997

[31] I. Abdo, T. Fujimura, T. Miura, K.K. Tokgoz, H. Hamada, H. Nosaka, A. Shirane, and K. Okada, in: *Proceedings of 2020 IEEE/MTT-S International Microwave Symposium (IMS)* (2020) pp. 623–626, https://doi.org/10.1109/IMS30576.2020.9224033

[32] M.M. Wiecha, R. Kapoor, A.V. Chernyadiev, K. Ikamas, A. Lisauskas, and H. G. Roskos, Antenna-coupled field-effect transistors as detectors for terahertz near-field microscopy, Nanoscale Adv. **3**, 1717–1724 (2021), https://doi.org/10.1039/D0NA00928H

[33] D. Čibiraitė-Lukenskienė, K. Ikamas, T. Lisauskas, V. Krozer, H.G. Roskos, and A. Lisauskas, Passive detection and imaging of human body radiation using an uncooled field-effect transistor-based THz detector, Sensors **20**(15), 4087 (2020), https://doi.org/10.3390/s20154087

[34] O. Momeni and E. Afshari, High power terahertz and millimeter-wave oscillator design: A systematic approach, IEEE J. Solid-State Circuits **46**(3), 583–597 (2011), https://doi.org/10.1109/JSSC.2011.2104553

[35] J. Grzyb, Y. Zhao, and U.R. Pfeiffer, A 288-GHz lens-integrated balanced triple-push source in a 65-nm CMOS technology, IEEE J. Solid-State Circuits **48**(7), 1751–1761 (2013), https://doi.org/10.1109/JSSC.2013.2253403

[36] J.V. Rudd and D.M. Mittleman, Influence of substrate-lens design in terahertz time-domain spectroscopy, J. Opt. Soc. Am. B **19**(2), 319–329 (2002), https://doi.org/10.1364/JOSAB.19.000319

[37] Proakis, *Digital Communications*, 4th ed. (McGraw-Hill Education, Boston, 2000).

KOMPAKTIŠKOS BELAIDĖS DUOMENŲ PERDAVIMO SISTEMOS SU ELEKTRONINIU THz ŠALTINIU IR DETEKTORIUMI KŪRIMAS

A. Cesiul [a], K. Ikamas [a, c], D.B. But [b], I. Morkūnaitė [a], T. Lisauskas [d], A. Lisauskas [a, b]

[a] *Vilniaus universiteto Taikomosios elektrodinamikos ir telekomunikacijų institutas, Vilnius, Lietuva*

[b] *Lenkijos mokslų akademijos Aukšto slėgio fizikos instituto CENTERA laboratorijos, Varšuva, Lenkija*

[c] *Generolo Jono Žemaičio Lietuvos karo akademijos Logistikos ir gynybos technologijų vadybos mokslo grupė, Vilnius, Lietuva*

[d] *MB „Terahercų Technologijos“, Vilnius, Lietuva*

Santrauka

Šiame straipsnyje pristatoma visiškai elektroninė belaidžio ryšio linija, veikianti 250 GHz dažniu. Pagrindiniai sukurtos sistemos elementai yra įtampa valdomas harmoninis osciliatorius, pagamintas naudojant 65 nm jungtinę metalo oksido puslaidininkio technologiją (JMOP), ir kvazioptinis detektorius su atrankiąja antena ir lauko tranzistoriumi, pagamintas naudojant 90 nm JMOP. Šaltinis atitaikytas trečiosios harmonikos spinduliuotės emisijai 252 GHz dažniu, jo spinduliuojama galia siekia –11 dBm lygį. Detektoriaus jautrio maksimumas yra 254 GHz, dažnių juostos plotis – 25 %, o minimali optinė efektinė triukšmo galia siekia 22 pW/$\sqrt{\text{Hz}}$. Duomenims koduoti naudojame moduliavimą įjungimo-išjungimo raktu ir demonstruojame skaitmeninio signalo perdavimą nuo 0,4 iki 18 m atstumu. Esant 0,4 m atstumui ir 32 MHz moduliacijos dažniui, pasiekiamas 15,9 dB signalo ir triukšmo santykis. Surinktos ryšio sistemos kanalo laidumas siekia 266 Mbit/s, tačiau jį riboja tik išoriniai elektroniniai komponentai – stiprintuvo ir moduliatoriaus dažnių juostos plotis. Įdiegus šiuolaikines aukšto dažnio grandines, laidumą būtų galima tiesiogiai padidinti iki 10 Gbit/s.